Impact of Rainfall Assimilation on High-Resolution Hydrometeorological Forecasts over Liguria, Italy

SILVIO DAVOLIO

Institute of Atmospheric Sciences and Climate, National Research Council, Bologna, Italy

FRANCESCO SILVESTRO

CIMA Research Foundation, Savona, Italy

THOMAS GASTALDO

University of Bologna, and Hydro-Meteo-Climate Service of ARPA Emilia-Romagna, Bologna, Italy

(Manuscript received 21 April 2017, in final form 27 June 2017)

ABSTRACT

The autumn of 2014 was characterized by a number of severe weather episodes over Liguria (northern Italy) associated with floods and remarkable damage. This period is selected as a test bed to evaluate the performance of a rainfall assimilation scheme based on the nudging of humidity profiles and applied to a convection-permitting meteorological model at high resolution. The impact of the scheme is assessed in terms of quantitative precipitation forecast (QPF) applying an object-oriented verification methodology that evaluates the structure, amplitude, and location (SAL) of the precipitation field, but also in terms of hydrological discharge prediction. To attain this aim, the meteorological model is coupled with the operational hydrological forecasting chain of the Ligurian Hydrometeorological Functional Centre, and the whole system is implemented taking operational requirements into account. The impact of rainfall data assimilation is large during the assimilation period and still relevant in the following 3 h of the free forecasts, but hardly lasts more than 6 h. However, this can improve the hydrological predictions. Moreover, the impact of the assimilation is dependent on the environment characteristics, being more effective when nonequilibrium convection dominates, and thus an accurate prediction of the local triggering for the development of the precipitation system is required.

1. Introduction

In the Mediterranean basin, many regions are frequently threatened by heavy precipitation events and floods, responsible every year for damage and loss of lives. High-impact weather due to rainfall exceeding 100 mm even within a few hours, and hourly intensities larger than 50–60 mm h^{-1}, are not uncommon in the region (Ramis et al. 2009; Ricard et al. 2012; Rebora et al. 2013). Therefore, improving the understanding and forecasting of such events has recently become a topic of great scientific interest, as demonstrated by several research projects and field campaigns [e.g., Hydrological Cycle in Mediterranean Experiment (HyMeX); Ducrocq et al. 2014] and publications (Buzzi et al. 2014; Scheffknecht et al. 2016; Davolio et al. 2016; Fiori et al. 2017; Lee et al. 2016; Duffourg et al. 2016; Röhner et al. 2016).

Being a coastal area characterized by complex orography that reaches high elevations within a few kilometers from the coastline (Fig. 1), the Liguria region in northern Italy is particularly prone to heavy precipitation episodes (Rebora et al. 2013; Faccini et al. 2015; Silvestro et al. 2016) that can severely affect urban areas, mostly located along the coast, in proximity of river outlets and sometimes even in the flat areas along the riverbeds. The steep topography and the particular morphology of the area, characterized by catchments of small dimensions (only a few are larger than 200 km^2) with very short response time, make rainfall predictions necessary to drive rainfall–runoff models in order to provide streamflow forecasts (Silvestro et al. 2015b). In fact, under these circumstances, the use of rainfall observations does not allow timely predictions.

The autumn 2014 was particularly severe for the Liguria region, and intense precipitation events developed in quick succession, sometimes even without a break.

Corresponding author: Silvio Davolio, s.davolio@isac.cnr.it

DOI: 10.1175/JHM-D-17-0073.1

Several flash floods occurred, including a devastating flood on 9 October (Silvestro et al. 2016), which caused hundreds of millions of euros in damage and one casualty in the city of Genoa. The latter was very similar to two other catastrophic events that occurred in 2011 and were deeply investigated (Silvestro et al. 2012; Rebora et al. 2013; Buzzi et al. 2014; Fiori et al. 2014): mesoscale convective systems, originating over the sea, affected a confined area inland with heavy and persistent rainfall that became devastating floods in a few hours in small watersheds. In general, the precipitation systems affecting Liguria often originate over the Mediterranean Sea, and the interaction with the orography may enhance rainfall intensity. These are usually characterized by short durations (12–36 h) and high intensities (Deidda et al. 1999; Boni et al. 2007). The polarimetric C-band radar that covers the region (location in Fig. 1b) is therefore a fundamental monitoring tool that captures the spatial structure and evolution of the precipitation systems moving toward the coast.

Despite the increase in resolution and improvements of numerical weather prediction (NWP) models (Clark et al. 2016), which are at present widely adopted operationally at convection-permitting scales (2 km or even less), accurate quantitative precipitation forecasts (QPFs) are still affected by uncertainties that are relevant at the fine spatial and temporal scales required for prediction of flash floods in catchments of such small dimensions (Siccardi et al. 2005; Cuo et al. 2011). Moreover, the forecasting skill for heavy precipitation associated with deep convection, which is frequently responsible for high-impact weather in the area of interest, is generally low, due to the chaotic behavior of convection dynamics that limits the intrinsic predictability. Errors in the initial and boundary conditions, as well as in the numerical models, may rapidly degrade the accuracy of QPFs. To produce a prediction that takes into account the whole forecast uncertainty, in the last few years several meteorological services have been running convection-permitting model (CPM) ensembles, varying the initial/boundary conditions or perturbing the model physics.

Different attempts have been taken to produce reliable QPFs from high-resolution NWP models. At short range (from a few hours to 12 h) QPF mainly depends upon the initial condition (Dixon et al. 2009; Clark et al. 2016), and thus a number of studies were devoted to assimilate observations, in particular rainfall data, into CPMs (Sun 2005; Dixon et al. 2009; Dow and Macpherson 2013), in order to improve forecast initialization. Recently, data assimilation and ensemble techniques have also been applied together to ingest radar reflectivity observations into CPMs (Bick et al. 2016). However, the assimilation of rainfall data is no easy task, because precipitation cannot be directly introduced into an NWP model. In fact, it is not a prognostic variable, but it is the result of complex dynamical and microphysical processes in the atmosphere. Among the assimilation methodologies applied to precipitation data, the nudging technique represents a simple, pragmatic, and empirical approach that lacks theoretical background, but has been proven to significantly improve QPFs, although with an impact limited to the first lead hours of model forecasts (Leuenberger and Rossa 2007; Stephan et al. 2008; Sokol 2009; Sokol and Zacharov 2012; Craig et al. 2012; Dow and Macpherson 2013; Bick et al. 2016). It is also very easy and computationally cheap and therefore suitable to be exploited in very short range hydrometeorological forecasting systems (Rossa et al. 2010). For these applications, radar rainfall estimates represent a promising data source for assimilation into high-resolution NWP models.

Craig et al. (2012) suggested that the impact of data assimilation depends on the characteristics of the meteorological environment. Two different dynamical regimes were identified based on the concept of convective equilibrium (Emmanuel 1994; Done et al. 2006), through the computation of the convective adjustment time scale (Done et al. 2006; Molini et al. 2011; Zimmer et al. 2011). Running an ensemble of high-resolution simulations for three different cases of convection over Germany, Craig et al. (2012) showed that latent heat nudging (Stephan et al. 2008), used to assimilate radar data, produces a more persistent correction to forecasts when convection is not constrained by large-scale forcing.

Within this framework, the present study is devoted to the extensive evaluation of a nudging procedure to assimilate radar rainfall estimates into the high-resolution CPM Modello Locale in Hybrid Coordinates (MOLOCH), included in a hydrometeorological forecasting chain. Unlike Craig et al. (2012), here the assessment is carried out over a relevant number (29) of deterministic forecasts by simulating all the precipitation events that occurred over Liguria during October–November 2014. The impact of the assimilation on QPFs is quantitatively evaluated using the structure, amplitude, and location (SAL) skill score (Wernli et al. 2008), an object-based measure that provides information on structure S, amplitude A, and location L of the precipitation field. Moreover, the impact of the assimilation is further evaluated in terms of hydrological response by coupling meteorological and hydrological models and using a probabilistic approach, as already discussed in Davolio et al. (2015). The analysis of assimilation results on a sufficiently large sample of deterministic forecasts and

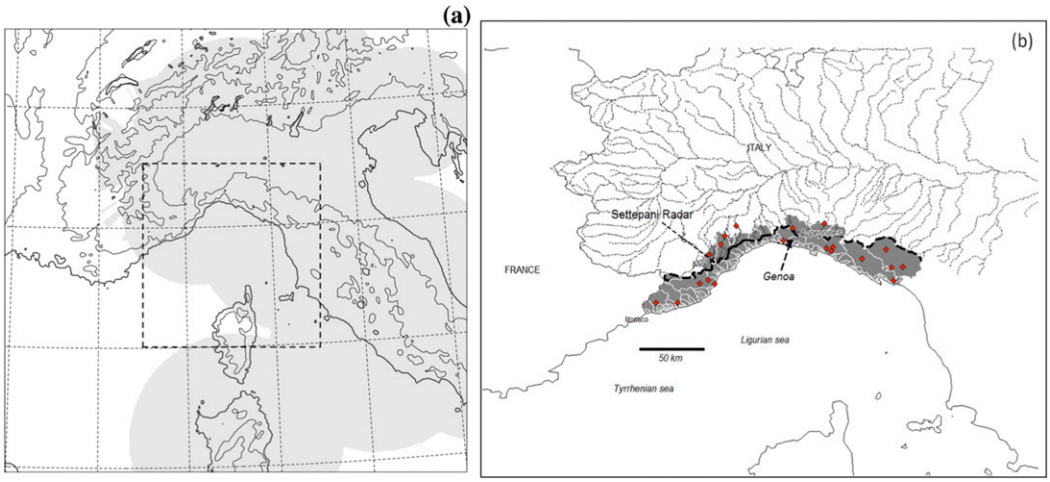

FIG. 1. (a) Coverage of the national radar mosaic (gray shading) drawn over the MOLOCH integration domain. MOLOCH orography (500 and 2000 m) is also plotted. The dashed box indicates the area used for the SAL and convective time-scale computations. (b) Liguria region of Italy: the main basins are shown in gray, and the black dotted line represents the watershed between the Tyrrhenian Sea and Po valley drainage direction. Location of the Doppler polarimetric C-band radar located on Mount Settepani (1386 m) is indicated. Red diamonds indicate the position of the closure sections of the 20 basins involved in the analysis.

events also allows us to explore the possible dependence of its impact on the convective time scale, as suggested by Craig et al. (2012). They also encouraged similar studies with different NWP models and data assimilation procedures in order to assess the sensitivity of their results to the modeling system, thus attaining more robust conclusions. Finally, the adopted procedure provides a practical evaluation of the QPFs, which can be relevant for operational hydrological application in the region, assessing how much the assimilation of the radar observations can improve the accuracy of QPFs at the catchment scale (Liu et al. 2013).

The paper is organized as follows. Section 2 presents the area of interest, the meteorological events, the components of the forecasting chain, and the methodologies, while the assimilation scheme is described in section 3. Results are discussed in section 4 from both meteorological and hydrological perspectives, and conclusions are drawn in section 5.

2. Data, models, and methodology

a. Area of interest and severe weather events

The Liguria region in northern Italy (Fig. 1) is characterized by steep orography (up to almost 2500 m height) and by basins whose drainage areas range between 10 and 1000 km^2, with rapid response time between 0.5 and 10 h. Most of the territory is covered by vegetation characterized by forest, meadows, and brushes, but the catchments mouth is often collocated with urbanized areas. The region is monitored by a meteorological network, named OMIRL, which is the official network managed by the regional Civil Protection Agency. It is part of the national network managed by the Italian Civil Protection Department (Molini et al. 2009). This network provides rain gauge measurements with 5–10-min frequency and counts about 150 instruments over the region, thus reaching an average density of 1 rain gauge per 40 km^2. The Liguria region is also covered by a Doppler polarimetric C-band radar located on Mount Settepani at 1386 m (Fig. 1b), which provides rainfall fields at 1 km $\times$ 1 km horizontal resolution and contributes to the national radar composite shown in Fig. 1a. Precipitation data for assimilation and verification are obtained by a merging of radar estimates and rain gauge measurements all over the model domain (see Fig. 1a for data coverage) with a method derived by Sinclair and Pegram (2005). This represents an operational rainfall product employed by the Liguria region hydrometeorological center.

For several days, from 8 to 13 October 2014, the synoptic circulation was favorable for persistent severe weather conditions over Liguria. Quite frequently in autumn, large-scale synoptic disturbances propagate and deepen in the Mediterranean basin. Southwesterly flow in the middle troposphere (Fig. 2a) was associated with warm and moist low-level advection that transports moisture toward the Ligurian coastal slopes exposed to southerly flows. Under these conditions, the Mediterranean Sea acted as a reservoir of humidity and heat, feeding low-level jets, and intense precipitation affected the region (Fig. 2d). In the first phase of the event,

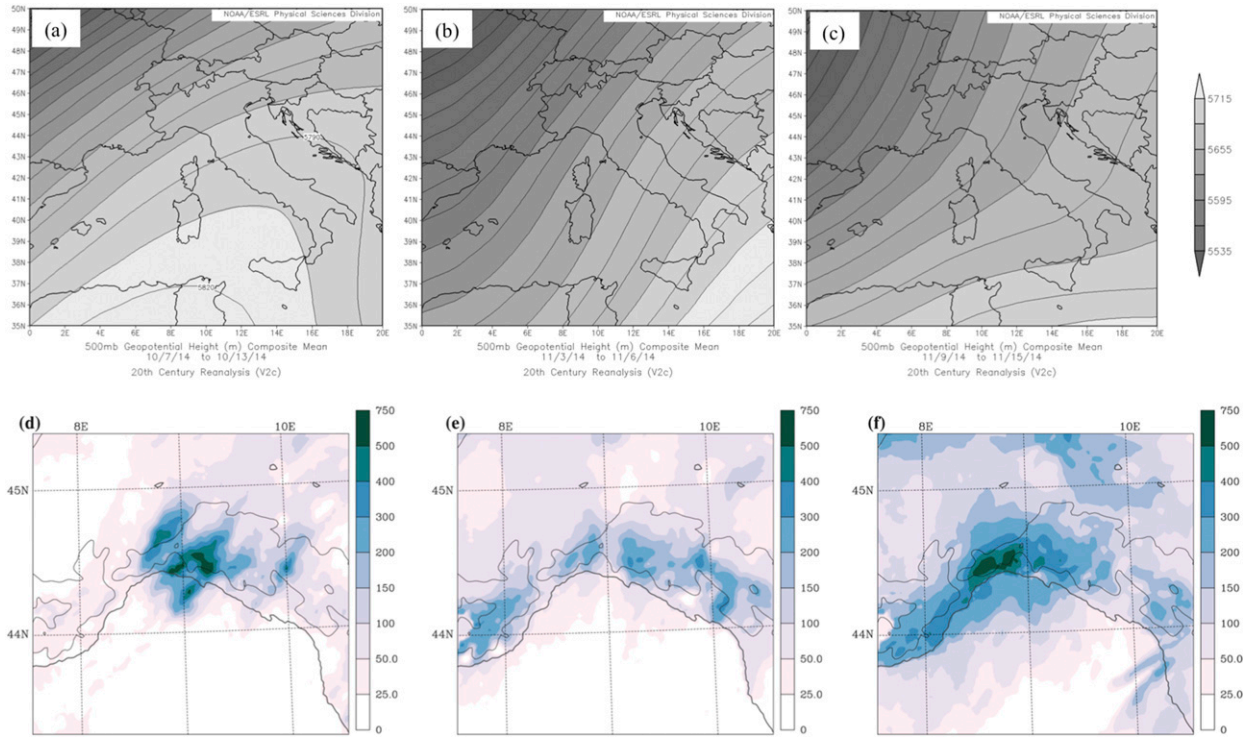

FIG. 2. Geopotential height (m) at 500 hPa (Twentieth Century Reanalysis) averaged for the periods (a) 7–13 Oct 2014, (b) 3–6 Nov 2014, and (c) 9–15 Nov 2014. (d)–(f) The total observed precipitation (mm) for the periods in (a)–(c), respectively.

rainfall was mainly associated with the development of quasi-stationary mesoscale convective systems (MCSs) in correspondence with lines of low-level wind convergence over the Ligurian Sea (as described in Buzzi et al. 2014; Fiori et al. 2017). While on 8 October rainfall (around 100 mm in 24 h) associated with several thunderstorms created peak flows in some basins over the central and eastern part of the region, the most intense phase was observed on 9 October. A V-shaped, backbuilding MCS produced rainfall amounts between 150 and 260 mm, with hourly peaks exceeding 100 mm (Fiori et al. 2017), leading to a total daily precipitation of almost 400 mm in the Bisagno catchment. As a consequence, the city of Genoa was flooded. Later, in the following days, thunderstorms developed in consecutive phases over both the sea and the mountains, fed by moist southerly flow. The severe weather episode ended with the passage of a cold front.

In November, similar large-scale circulation patterns led to two consecutive severe weather periods on 3–6 November (Fig. 2b) and 9–15 November (Fig. 2c). During the first period, a deep trough elongated over the Mediterranean and northern Africa and an intense Mediterranean cyclone developed. Strong, moist, low-level southerly flow (southwesterly aloft) supported widespread heavy rainfall, attaining almost 200 mm in 72 h over most of the territory (Fig. 2e). Local floods were reported. During the second period, precipitation systems were mainly convective and sometimes organized in stationary MCSs, responsible for further exceptional amounts of rainfall (Fig. 2f), exceeding 200 mm in 24 h in several locations and largely exceeding 200 mm in 96 h the entire region. Critical hydrogeological consequences were reported together with two casualties. After a very short break, an Atlantic cyclone moving over France drove an intense frontal system over Liguria, with again heavy precipitation on 14–15 November. Rainfall up to 300 mm in 24 h locally, and more than 200 mm in 48 h over a wide area, produced widespread flooding in urban areas and overflow of several minor watersheds. Finally, a weak cyclonic circulation over the Mediterranean in the last week of the month was able to support two further intense precipitation events on 25 and 28 November, mainly associated with intense southerly flow and sharp convergence lines over the Gulf of Genoa.

b. NWP system and model setup

Meteorological forecasts are based on the Bologna Limited Area Model (BOLAM) and MOLOCH models

employed in cascade (one-way nesting). Both models are developed at the Institute of Atmospheric Sciences and Climate (ISAC) of the National Research Council (CNR) of Italy, and their application has been thoroughly described in recent papers (Buzzi et al. 2014; Davolio et al. 2017). BOLAM (Buzzi et al. 2003) is a primitive equation, hydrostatic model with parameterized convection (Kain 2004). In the present application, it is driven by IFS–ECMWF forecasts and is employed with a horizontal resolution of 8.3 km to provide the lateral boundary conditions for MOLOCH at hourly frequency. MOLOCH (Malguzzi et al. 2006; Buzzi et al. 2014) is a nonhydrostatic, fully compressible, convection-permitting model, which employs a hybrid terrain-following coordinate, depending on air density and relaxing smoothly to horizontal surfaces away from Earth's surface. MOLOCH is run at 2.3-km horizontal resolution, using 50 vertical levels. Time integration is based on an implicit scheme for the vertical propagation of sound waves, while explicit, time-split schemes are implemented for integration of the remaining terms of the equations of motion. Three-dimensional advection is computed using the Eulerian weighted average flux scheme (Billett and Toro 1997). BOLAM and MOLOCH share the same parameterization schemes for radiation (Ritter and Geleyn 1992; Morcrette et al. 2008), turbulence (*E-l* 1.5-order closure; Zampieri et al. 2005), soil processes, and microphysics, as described in more detail in Davolio et al. (2017). In accordance with the operational setup of the modeling chain implemented at CNR-ISAC, in the present application MOLOCH simulations are initialized with a 3-h BOLAM forecast in order to avoid a downscaling based on pure interpolation from the global model. The list of MOLOCH integrations, performed to simulate all the severe weather events, is provided in Table 1. The integration domain of MOLOCH is shown in Fig. 1a. For each event, one MOLOCH control simulation (CNTR) and one simulation with assimilation (NUDG) are performed, starting from the same initial conditions. Data assimilation is not applied in BOLAM.

TABLE 1. Initialization dates and hours of the MOLOCH simulations.

Initialization date	Initialization hour (UTC)
7 Oct 2014	0300, 1500
8 Oct 2014	0300, 1500
9 Oct 2014	0300, 1500
10 Oct 2014	0300, 1500
11 Oct 2014	0300, 1500
12 Oct 2014	1500
13 Oct 2014	1500
3 Nov 2014	0300, 1500
4 Nov 2014	0300, 1500
5 Nov 2014	0300, 1500
6 Nov 2014	0300
9 Nov 2014	1500
10 Nov 2014	0300, 1500
11 Nov 2014	0300, 1500
12 Nov 2014	0300
15 Nov 2014	0300
17 Nov 2014	0300
25 Nov 2014	0300
28 Nov 2014	0300

c. *The Continuum hydrological model*

Continuum [for a detailed description, refer to Silvestro et al. (2013, 2015a)] is a continuous distributed hydrological model that strongly relies on a morphological approach, based on a novel way for identification of the drainage network components (Giannoni et al. 2005). The model has been conceived to be a compromise between models with a strong empirical connotation, which are easy to implement but far from reality, and complex physically based models, which try to reproduce the hydrological processes with high detail but that introduce complex parameterization and consequent uncertainty and lack of robust parameter identification. All of the main hydrological phenomena are modeled in a distributed way. The basin is represented using a regular square mesh, based on a digital elevation model (DEM), and the flow directions are identified on the basis of the directions of maximum slope derived from the DEM.

For the current application, the model is implemented with a spatial resolution of 0.005° (about 480 m) based on the Shuttle Radar Topographic Mission (SRTM) DEM. The temporal resolution used in all the experiments is hourly. Meteorological input is generated interpolating gauge data of temperature, radiation, humidity, and wind speed. Rainfall fields are obtained by merging radar estimates and rain gauge measurements (Sinclair and Pegram 2005).

The Continuum model has six parameters that require calibration at the basin scale: two for the surface flow (u_h and u_c), two for the subsurface flow (c_t and c_f), and two for deep flow and water table (V_{Wmax} and R_f) processes. The parameters were calibrated mainly with the objective of reproducing peak flow values and time of peak, minimizing the relative error of high flows (REHF). It was possible to calibrate the model for 11 sections and for the period from 1 January 2013 to 31 December 2014, using some standard statistics as described in the appendix. The values of the statistics for the calibration period are reported in Table 2. In basins where it was not possible to make the calibration, average values of the parameters obtained by the calibration process are assumed.

TABLE 2. NS and REHF for the discharge simulations by Continuum model driven by observations, after calibration of the parameters for different basins and sections.

Basin	Section	NS	REHF
Magra	Calamazza	0.81	0.14
Vara	Nasceto	0.83	0.10
Entella	Panesi	0.77	0.18
Bisagno	Passerella Firpo	0.26	0.16
Neva	Cisano	0.71	0.25
Arroscia	Pogli	0.74	0.31
Argentina	Merelli	0.84	0.21
Bormida	Murialdo	0.35	0.51
Bormida	Piana Crixia	0.76	0.41
Orba	Tiglieto	0.88	0.21
Aveto	Cabanne	0.73	0.41

The comparison between the forecasts forced by rainfall predictions obtained with and without the data assimilation in MOLOCH is carried out over 20 sections located in the considered domain and with areas ranging between 100 and 1600 km^2.

d. The RainFARM model

RainFARM (Rebora et al. 2006) is a stochastic rainfall downscaling model used for generating an ensemble of precipitation fields that are consistent with large-scale predictions issued by meteorological models (Laiolo et al. 2014) and/or by expert forecasters (Silvestro et al. 2011). It can reproduce the small-scale variability of precipitation needed to correctly drive the rainfall–runoff model. RainFARM accounts for the spatial–temporal variability of precipitation fields at scales smaller than those at which reliable QPFs are available. RainFARM preserves the information at large-scales derived from a QPF and is able to generate small-scale structures of precipitation that are consistent with radar observations of midlatitude precipitation events.

The basic idea is that the spatial–temporal Fourier spectrum of the precipitation field, estimated at large scale from a meteorological model prediction, follows the functional form

$$|\hat{g}(k_x, k_y, \omega)|^2 \propto (k_x^2 + k_y^2)^{-\alpha/2}\omega^{-\beta},$$

where k_x and k_y are the x and y spatial wavenumbers and ω is the temporal wavenumber (frequency), whereas α and β represent two parameters of the model that are estimated from the power spectrum of precipitation predicted by an NWP model on the wavenumbers/frequencies that correspond to the spatial–temporal scales at which the meteorological model prediction is considered reliable.

To use the model, it is necessary first to define the reliable spatial and temporal scales of the NWP model ($S_{\rm rel}$ and $T_{\rm rel}$). Then, the downscaled rainfall fields are forced to preserve both the spatial–temporal patterns and the precipitation volume at these scales. In this application the downscaling is applied to the MOLOCH model. Since the analysis is aimed at reproducing discharge peaks in a probabilistic sense, rather than to mimic the timing of streamflow, as in Davolio et al. (2015), we assume $S_{\rm rel} = 15$ km and $T_{\rm rel} = 6$ h. Although the temporal scale of aggregation is 6 h, the final downscaled field has hourly resolution.

e. Hydrometeorological chain

The hydrometeorological chain is made by the cascade of the NWP model (MOLOCH), the stochastic downscaling model (RainFARM), and the hydrological model Continuum (Davolio et al. 2015; Silvestro et al. 2011). The output is made by an ensemble of streamflow scenarios and in the present application the number of members is set to $N = 100$. Since streamflow observations are available only for a limited number of stations, and in order to avoid possible errors introduced by hydrological modeling, the streamflow simulations obtained by Continuum forced with observed meteorological variables are used as ''reference hydrographs''; this is a common and widely used approach (Berenguer et al. 2005; Borga 2002; Vieux and Bedient 2004). The run of the hydrological model is carried out for the period from 1 January to 31 December 2014 in order to avoid spinup problems at the beginning of the analyzed period, which starts in October 2014.

f. Skill scores used for meteorological and hydrological verification

In addition to a qualitative evaluation of the forecasts through a visual comparison between meteorological fields, a quantitative assessment of rainfall prediction is carried out. To avoid the well-known limitations of traditional measures of skill for convection-permitting models (the double-penalty problem above all; Rossa et al. 2008), an object-based approach is used, based on the SAL technique (Wernli et al. 2008). Individual objects in the accumulated precipitation fields are identified (as continuous areas of grid points exceeding a selected threshold) and compared, providing information about structure S, amplitude A, and location L errors of QPF. Therefore, SAL indicates whether the observed rainfall is over-/underestimated, if the structure of the precipitation objects is too sharp/flat or too broad/small, and if they are correctly located with respect to the observations. A perfect match between a forecast and observations would result in $S = A = L = 0$. It is worth mentioning that SAL has to be computed on a

meaningful domain to correctly verify QPF. It is recommended (Wernli et al. 2009) to use a domain not larger than $500 \times 500\,\text{km}^2$. In fact, if the domain is too large, it encompasses different meteorological systems, and the comparison could be not representative.

For hydrological prediction verification, the continuous rank probability score (CRPS; Stanki et al. 1989) measures the distance between the predicted and the observed cumulative distribution functions (CDFs) of scalar variables. It is defined as

$$\text{CRPS} = \int_{-\infty}^{+\infty} [F(x) - H(x - X_r)]^2\, dx,$$

where $F(x)$ is the CDF of the hydrological ensemble, X_r is the observed (or in general the reference) variable, and $H(x - X_r)$ is the CDF of observations that is, at the end, a step-shaped function with value 1 for $x \geq X_r$ and 0 for $x < X_r$. Hersbach (2000) proposed a reliability–resolution–uncertainty decomposition of the CRPS useful for hydrological applications. CRPS = 0 means a perfect match between observations and simulation while an increasing CRPS means a progressively larger distance between observations and forecast. Thus, although CRPS is very useful, the dependence on magnitude of the data reference makes spatial comparisons across catchments difficult. To overcome this limitation, Trinh et al. (2013) proposed a variant of this score, that we call here reduction CRPS (RCRPS), by dividing the CRPS by the standard deviation of the observations σ_0 (or reference values) obtained for each hydrological station over the analyzed time period.

3. The assimilation scheme

Rainfall assimilation is performed using a nudging scheme originally developed for BOLAM (Davolio and Buzzi 2004). This scheme was applied to large-scale precipitation systems and to a model with parameterized convection. It demonstrated that it was able to improve the QPF for several heavy precipitation events and to effectively modify the structure and properties of baroclinic unstable modes (Buzzi and Davolio 2007) when applied to a conceptual model of midlatitude cyclogenesis. However, as for similar nudging schemes (e.g., latent heat nudging), its applicability at the convective scale is by no means guaranteed (Dixon et al. 2009). In the present study, the nudging scheme is adapted and applied to MOLOCH for the first time, therefore requiring validation and tuning.

The scheme modifies the model humidity profiles at each grid point where observations are available, depending on the comparison between observed and forecast rainfall. Hourly rainfall data (described in section 2a), interpolated on the MOLOCH grid, are assimilated. The nudging adjustment progressively increases (decreases) specific humidity toward oversaturation (undersaturation) if the model underestimates (overestimates) rainfall, following the equation

$$\frac{\partial q(k)}{\partial t} = -\frac{\nu(k)}{\tau}[q(k) - \varepsilon^{\pm} q^*(k)]\sqrt{|P_{\text{diff}}|},$$

where $q(k)$ is the model specific humidity profile defined at each model level k; $q^*(k)$ is the specific humidity profile at saturation; τ is a relaxation time; $\nu(k)$ is a vertical modulation profile, whose value may vary between 0 and 1; $\varepsilon^{\pm}$ is the over-/undersaturation coefficient; and P_{diff} is the difference between observation and model precipitation (nudging is activated only if $|P_{\text{diff}}|$ is larger than $1\,\text{mm}\,\text{h}^{-1}$). The main role of the parameter $\nu(k)$ is to limit the specific humidity adjustment in the boundary layer, in order to avoid too unstable profiles that can produce excessive convective activity. Within each 1-h interval and assuming a linear evolution for the observations, forecast and observed rainfall are progressively accumulated every time step and then compared. Therefore, P_{diff} is the difference between rainfall accumulated up to the current time step, expressed in millimeters per hour.

An extensive preliminary phase was devoted to define optimal coefficients for the scheme. Several heavy precipitation events were simulated (not only those of 2014) with and without data assimilation, and forecast skill was quantitatively evaluated using skill scores (e.g., equitable skill score, false alarm rate, probability of detection) and comparing the meteorological fields. Final selected values for the coefficients are summarized in Table 3.

Data assimilation is performed during the first 6 h of the MOLOCH simulation, that is, between 0300 and 0900 UTC (between 1500 and 2100 UTC) for the simulations initialized with 0000 (1200) UTC global analysis. This setup is thus compatible with an envisaged operational implementation for short-range forecasts, taking into account the global data delivery time and requirements for collection and processing the observations.

Among the numerous experiments performed in the preliminary phase, it is worth mentioning some sensitivity tests concerning the impact of the observation frequency and the length of the assimilation period. In the first case, the use of 10-min accumulated rainfall, instead of hourly data, associated with a consistently reduced relaxation time, turned out to be slightly beneficial during the assimilation period, but did not improve, or even worsened, the results of the following free forecast. This result is in contrast with some previous data assimilation studies

TABLE 3. Selected coefficients for the nudging equation. Parameters ε^+ and ε^- are the over- and undersaturation factors, respectively; z is the elevation above the sea level; $\nu(k)$ is the vertical modulation profile; and τ is the relaxation time.

Nudging coefficient	Value
ε^+	1.02
ε^-	0.95
$\nu(k)$	0, for $z > 8000$ m
	$(8000 - z)/3000$, for $5000 < z < 8000$ m
	1, for $2000 < z < 5000$ m
	$(z/2000)^{0.2}$, for $0 < z < 2000$ m
τ	15 min

(e.g., Leuenberger and Rossa 2007; Stephan et al. 2008) that used radar data at very high temporal resolution (few minutes) as reference; however, it interestingly confirms the recent finding of Bick et al. (2016) that although less frequent updates of radar observations produce a less accurate analysis, it leads to a more balanced model state and thus better forecasts.

In the second set of experiments, a 3-h assimilation window (instead of 6 h) was tested, since it represents a more suitable option in view of an operational implementation. The selection of the assimilation interval is an interesting issue not only for nudging schemes (Liu et al. 2013). All the simulations listed in Table 1 were performed with this configuration, but the impact of the assimilation was less positive during the free forecast than with a 6-h assimilation window. This is possibly because, within the 3 h of assimilation, rainfall observations are not able to provide sufficient information to trigger the precipitation system: convective systems may develop very quickly, without preceding rainfall in the surrounding region, thus without suitable data to be assimilated. The presence of rainfall is in fact a necessary condition for this assimilation scheme. Moreover, the model requires a longer nudging period to retain the assimilated information more efficiently.

4. Results

The performance of the assimilation is first discussed in terms of accuracy of meteorological forecasts. In particular, 3-hourly accumulated precipitation is statistically evaluated using the SAL verification method. Then, the impact on hydrological predictions is evaluated.

a. *Meteorological evaluation of the assimilation scheme*

To compute SAL, it is necessary to define a rainfall threshold in order to identify precipitation objects in the analysis domain (shown in Fig. 1a). In the present application, instead of using a threshold value dependent on the maximum rainfall attained in the domain, as originally suggested by Wernli et al. (2008), two different thresholds, 1 and 5 mm (for 3-h precipitation), are subjectively selected, as done in previous studies (e.g., Sokol and Zacharov 2012). SAL is then computed for both thresholds: the first is aimed at evaluating the entire precipitation field, while the second considers only rainfall of relevant intensity. Higher threshold values would have excessively reduced the number of points for the computation, thus limiting the statistical significance of the results.

SAL plots concerning the precipitation accumulated in the first 3 h of the free forecast (after the 6-h assimilation period) are shown in Fig. 3. Every simulation is represented by a dot in the graph. Forecast errors in terms of structure S and amplitude A are reported on the x and y axes, respectively, while the color of the dots denotes the location accuracy L. It is worth recalling that a perfect forecast would produce a red dot in correspondence of the axis origin. The gray rectangle identifies the S and A interquartile range. The evident reduction of the rectangle area in the assimilation experiments with respect to the CNTR runs, for both the thresholds, is a clear indication of a general improvement in QPF. Moreover, a remarkable reduction of outliers (particularly wrong forecasts) is attained when the nudging is applied.

Considering SAL results for the 1 mm threshold (Figs. 3a,b), the value of S indicates a general tendency for the CNTR simulations to produce too small and too peaked precipitation objects (Wernli et al. 2009), while the nudging is able to correct this error. However, nudging tends to produce a slight overestimation of the rainfall intensity, as also highlighted by the A median. The L component is strongly improved as the number of red/yellow dots increases in the SAL plot for the NUDG simulations. Moreover, blue dots, which are those indicating largely misplaced QPF, disappear.

With the 5-mm threshold (Figs. 3c,d), CNTR simulation dots are mostly located in the first and third quadrants of the plot. This indicates precipitation objects that are either too intense and wide or too weak and sharp. Consequently, the S and A interquartile range is wide, as shown by the gray box. Median values for S and L are close to 0 due to compensation between the errors rather than to an accurate QPF. The SAL plot for the NUDG experiments confirms a general improvement. Results in terms of S and A are less widespread, and the L component is also improved.

To evaluate the nudging impact during the whole forecast, for each simulation and at different lead times, the difference between the absolute value of each SAL component of the CNTR run and of the NUDG run is

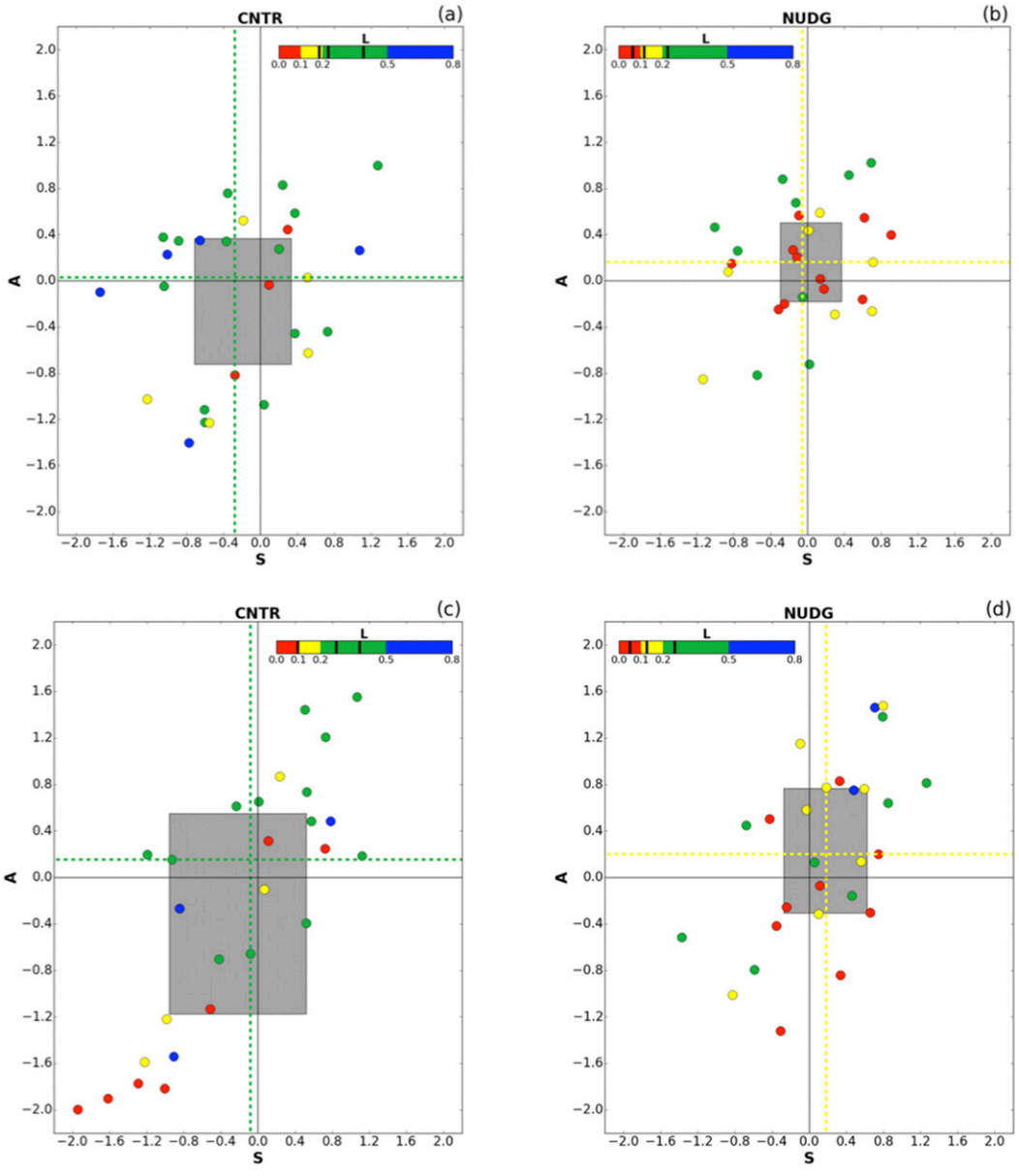

FIG. 3. SAL plots computed for 3-hourly accumulated precipitation, for rainfall thresholds of (a),(b) 1 mm and (c),(d) 5 mm for (left) CNTR runs and (right) NUDG simulations. Forecasts are in the range between +6 and +9 h, that is, during the first 3 h of the free forecast after the assimilation period. Each dot refers to a simulation; dot color indicates the value of L as in the legend. The two dashed lines indicate the medians of A and S, and the gray box identifies the S and A interquartile range. The median and first and third quartile values for L are indicated as black segments over the L legend. The value of the median of L determines the color of the dashed lines.

computed (e.g., for S: $|S_{\text{cntr}}|-|S_{\text{nudg}}|$), considering the precipitation accumulated over 3-h intervals. Thus, a positive value of the difference indicates an improvement due to assimilation for the SAL component considered. Unfortunately, the information on the type of error is lost in this way, since only its magnitude is considered (e.g., for A, an overestimation cannot be distinguished from an underestimation, since the absolute value of A is considered). However, this procedure provides a very intuitive picture of the nudging performance, as shown in Fig. 4.

For both thresholds, QPF is largely improved during the period of assimilation. This is not particularly relevant for the present operational-oriented application, but indicates a positive impact of the nudging scheme that could be useful for reanalysis purposes. For

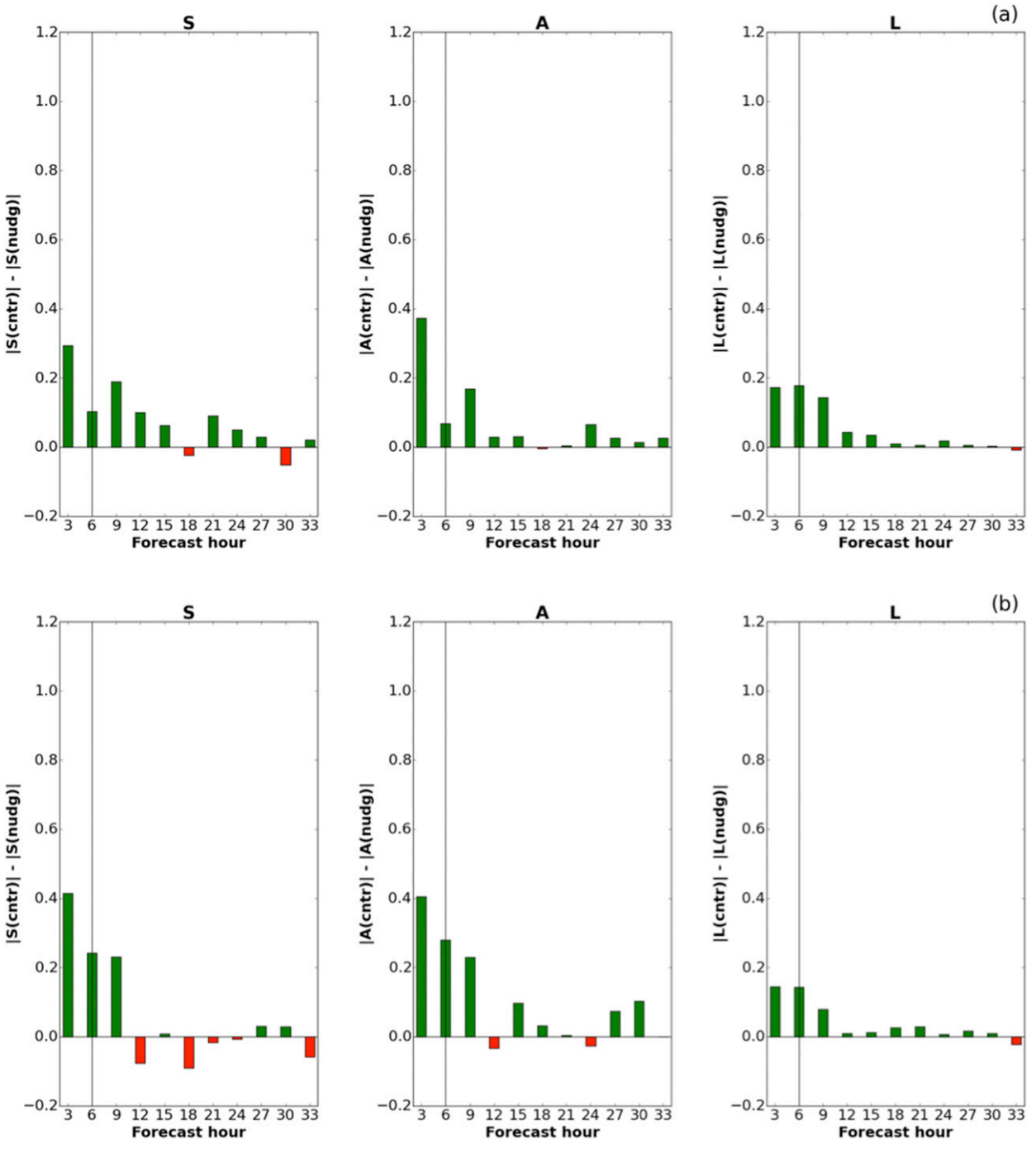

FIG. 4. Averaged impact of the nudging with respect to the forecast lead time, computed for all the events and for two 3-h rainfall thresholds, (a) 1 mm and (b) 5 mm, in terms of the differences between the absolute values of each SAL component in the CNTR and in the NUDG experiments. Positive (negative) values in green (red) indicate an improvement (worsening) of the QPF in the assimilation experiments. The vertical line in correspondence to the 6-h forecast indicates the end of the assimilation period.

nowcasting and short-range prediction, it is relevant that the QPF improvement due to rainfall assimilation lasts beyond the assimilation period, especially for low threshold values. There is a systematic improvement in the first 3 h of the free forecast, but the positive impact decays quite rapidly at longer lead times.

With the aim of obtaining more detailed information on the nudging effectiveness and even to identify

"good" and "bad" examples of forecasts, events of October and November are analyzed separately. The SAL plots (Fig. 5) clearly indicate that the CNTR forecasts concerning the October events are affected by relevant errors: precipitation is largely underestimated, with 6 out of 10 forecasts characterized by a value of A lower than -1.5, corresponding to an error larger than 85%. Also, S is negative, indicating too small and too sharp objects in the predicted field, while the location is a much better forecast. The rainfall assimilation remarkably improves QPF during the first 3 h of the free forecast for all the SAL components, especially in terms of amplitude and structure.

Conversely, the CNTR predictions are more skillful for the events of November, with only a slight tendency to overestimate the rainfall amount. In these conditions, the assimilation does not produce any extraordinary effects. Nudging slightly accentuates the overestimation, but definitely improves the forecast in terms of location. In general for both months, forecasts with assimilation outperform the CNTR runs, since the amplitude of the gray box is reduced and the box is closer to the axis origin (or at least at the same distance).

The impact of the assimilation during the whole forecast is analyzed for the two months separately in Fig. 6, which shows the difference between the absolute value of each SAL component of the CNTR and of the NUDG experiments. For the events of October, rainfall assimilation greatly improves forecasts in terms of intensity, structure, and location of the precipitation objects, during the assimilation period and also in the first hours of the free forecast. However, for lead times between 4 and 6 h, the impact progressively vanishes. Conversely, for November events the positive impact of the assimilation is largely reduced and even a slight degradation of the predictions in terms of amplitude is obtained. However, as for the previous month, a positive and persistent improvement is attained for the rainfall location.

These results point out a different behavior of the meteorological forecasts and of the assimilation scheme between the two analyzed periods. The October 2014 events are characterized by a lower predictability, and the forecast skill is low (Fig. 5a). Rainfall assimilation through nudging of the humidity profile demonstrates the ability to largely improve predictions at least within the first 3 h of the free forecast and, only for some events, up to 6 h. November events seem more predictable, and the forecasts are more skillful (Fig. 5c). The data assimilation impact is weak and does not last during the free forecast, except in terms of localization. Given the results of Craig et al. (2012), the following section is aimed at investigating if this different behavior can be related to different characteristics of the meteorological events.

b. *Characteristics of the meteorological environment*

Data assimilation applied to convection-permitting models statistically improves forecast accuracy, but not every case presents a dramatic and positive benefit (Clark et al. 2016). Craig et al. (2012) showed that the impact of radar rainfall assimilation is constrained by the environment characteristics, defined in terms of the presence of convective equilibrium (Emmanuel 1994). Two different meteorological regimes are defined. When convection is in equilibrium with the large-scale forcing, it consumes the instability [convective available potential energy (CAPE)] at the same rate instability is continuously generated by the large-scale forcing. Under these conditions, convection mean properties are set by the environment, and the location, intensity, and size of the precipitation is determined by the large-scale flow. Usually convective inhibition (CIN) values are approximately zero. This corresponds to equilibrium convection. On the other hand, nonequilibrium convection (or triggered convection; Zimmer et al. 2011) is characterized by weak synoptic forcing and a strong inhibition to the release of conditional instability. Therefore, large values of CAPE build up due to the presence of a relevant capping inversion. Precipitation is strongly modulated by mesoscale thermodynamics, in particular by the exact timing and location of where the local triggering is able to overcome the inhibition barrier (CIN). When this occurs, CAPE is rapidly exhausted. The two regimes are associated with different practical predictability, with nonequilibrium convection being less predictable since it depends upon local processes, which are usually hard to predict. They can be disentangled by computing the convective time scale defined as

$$\tau_c = \frac{\mathrm{CAPE}}{d\mathrm{CAPE}/dt} = \frac{1}{2}\frac{C_p \rho T_0}{L_v g}\frac{\mathrm{CAPE}}{P},$$

where C_p is the air specific heat at constant pressure, ρ is the air density, T_0 is a reference temperature value, L_v is the latent heat of evaporation, g is the acceleration due to gravity, and P is the precipitation rate. Short (long) convective time scales are typical of equilibrium (nonequilibrium) convection. It is not possible to define a sharp threshold between the two regimes. Previous studies (Keil and Craig 2011; Molini et al. 2011; Zimmer et al. 2011) indicate a threshold in the range between 6 and 12 h, although it is more meaningful to analyze possible changes in magnitude among different analyzed events, instead of taking τ_c at face value (Keil et al. 2014).

The convective time scale τ_c is evaluated over the same domain employed for SAL (Fig. 1a), since the

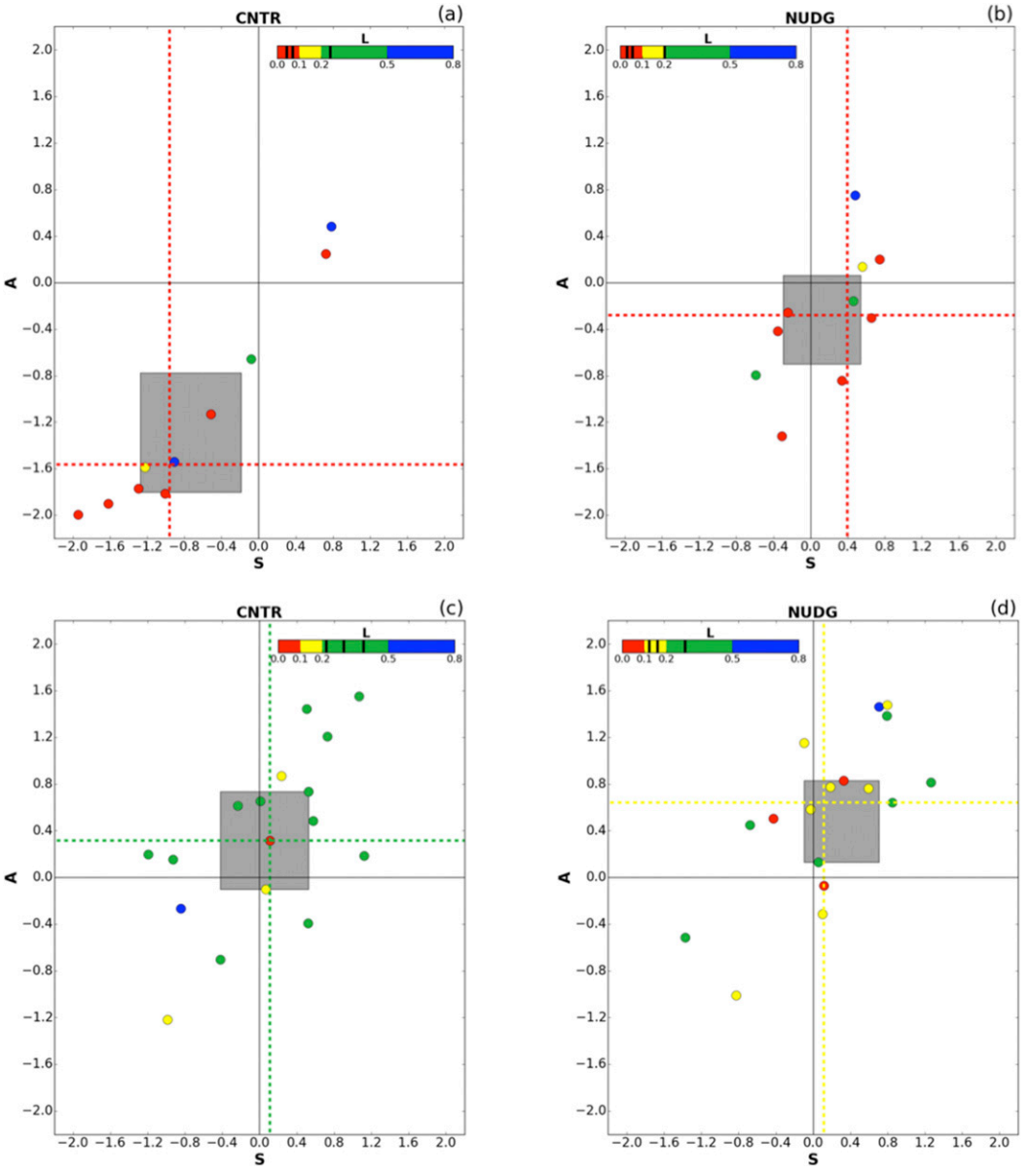

FIG. 5. As in Fig. 3, but considering separately the heavy precipitation events that occurred in (a),(b) October and (c),(d) November, and for the rainfall threshold of 5 mm.

aim is to focus on the precipitation systems affecting the Liguria region and close surrounding areas. Moreover, this allows us to directly relate the verification results (SAL) with environment characteristics. Time scale τ_c is computed using CAPE provided hourly by MOLOCH output and hourly precipitation from observations (merging between radar estimates and rain gauge measurements, as described in section 2). Rainfall and CAPE are smoothed using a Gaussian filter in order to remove the local variability associated with single convective cells. Several sensitivity tests were preliminarily performed to evaluate the impact of the smoothing parameters and of the selection of the rainfall threshold defining rain/no-rain areas on the τ_c computation. A value of 25 km for the Gaussian standard deviation and a threshold of $1\,\mathrm{mm\,h^{-1}}$ were selected.

Values of τ_c computed for all the analyzed events are shown in Fig. 7. Although there is some variability even within a single event, especially for the episodes that occurred in October, a clearly larger convective time scale is attained in October, whereas for the November events, τ_c hardly exceeds the value of 10 h. The mean values of the two months confirm different dynamical

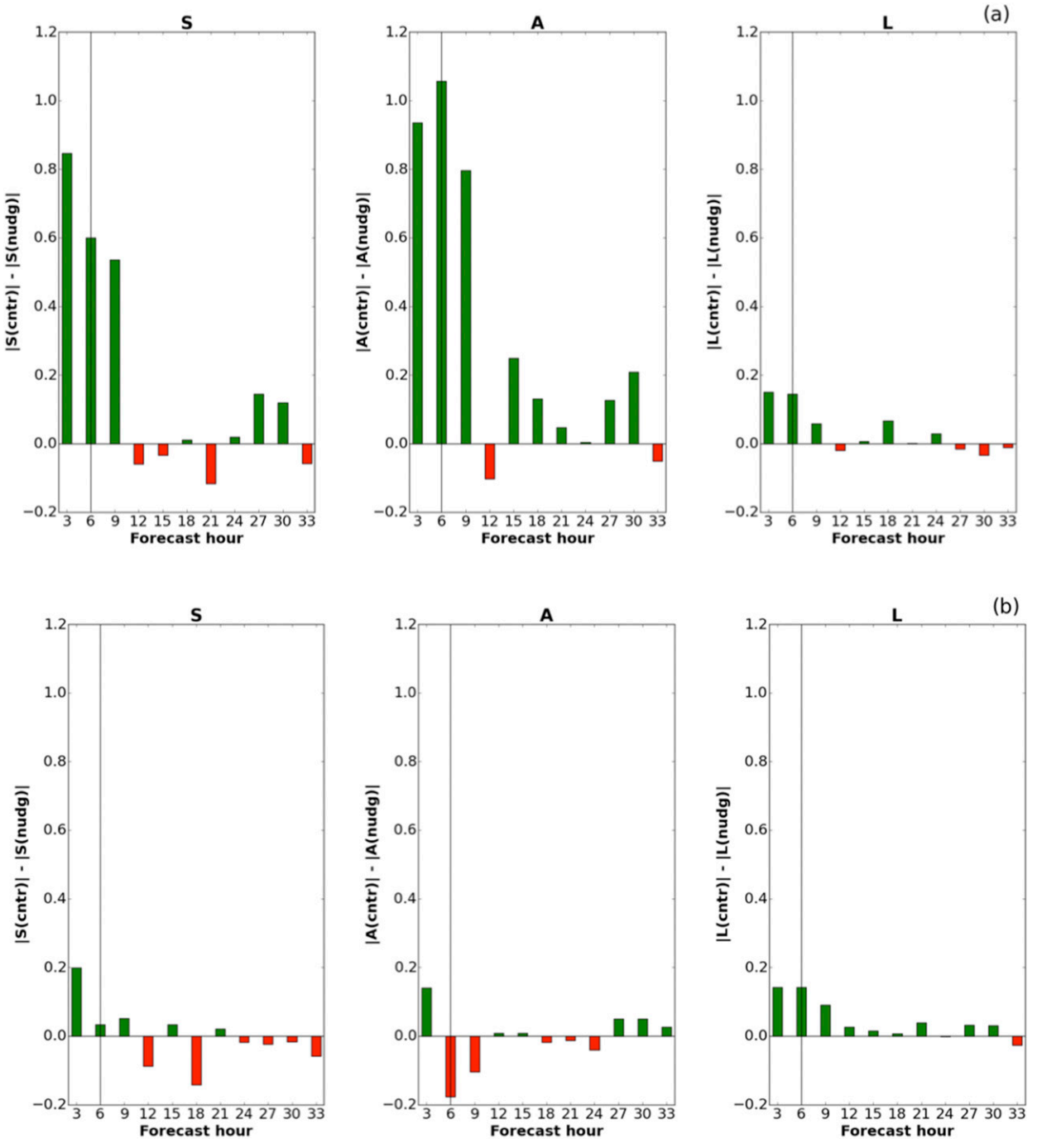

FIG. 6. As in Fig. 4, but considering separately the heavy precipitation events that occurred in (a) October and (b) November, and for the rainfall threshold of 5 mm.

regimes. This agrees with observational evidence (as also described in section 2a): October was mainly characterized by the development of isolated and stationary MCSs, such as the one responsible for the Genoa flood on 9 October. In particular, the latter event was classified as nonequilibrium convection in a recent meteorological study by Fiori et al. (2017), in agreement with our findings.

The above analysis supports the results obtained with the CNTR simulations, which display a lower practical predictability (Keil et al. 2014), and thus worse scores, for the weakly forced weather regimes in October. Moreover,

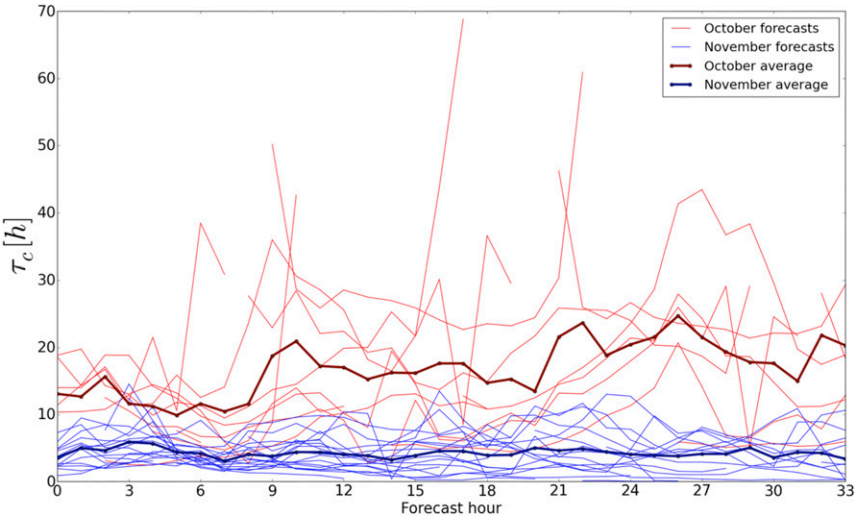

FIG. 7. Values of the convective time scale τ_c computed for the events of October (red lines) and November (blue lines), as a function of the forecast range. The two bold lines represent the average values of τ_c for the two months.

the behavior of τ_c is consistent with the different impacts of the rainfall assimilation, as proposed by Craig et al. (2012). In fact, in October, average conditions of non-equilibrium convection imply the presence of strong CIN. To obtain an accurate forecast, it is thus critical for the model to correctly simulate the timing and location of the trigger needed to locally overcome the inhibition threshold. The assimilation is able to provide the appropriate trigger and thus to markedly improve the QPF. Once the trigger is provided, long-lived convective

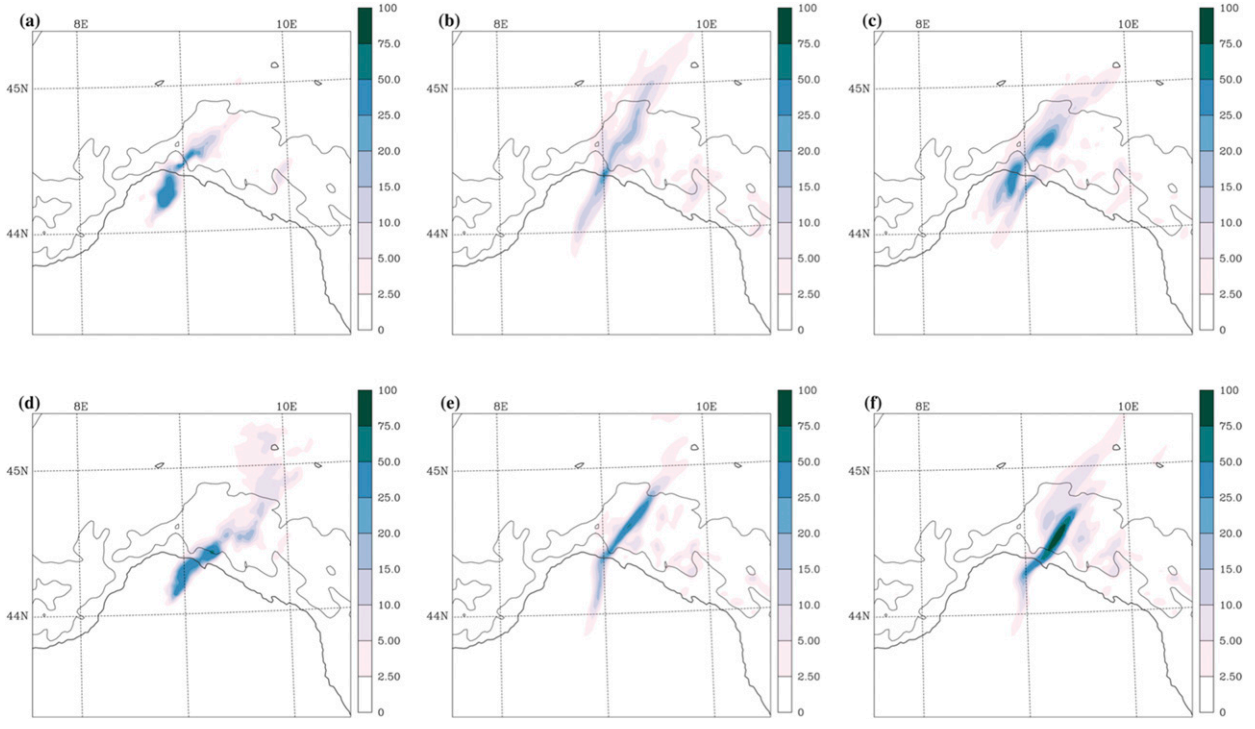

FIG. 8. Shown is hourly precipitation (mm) at 0900 UTC 9 Oct 2014 that corresponds to the end of the assimilation period from (a) observations (radar and rain gauges), (b) CNTR simulation, and (c) NUDG experiment and hourly precipitation (mm) at 1200 UTC 9 Oct 2014 that corresponds to the third hour of the free forecast from (d) observations, (e) CNTR, and (f) NUDG.

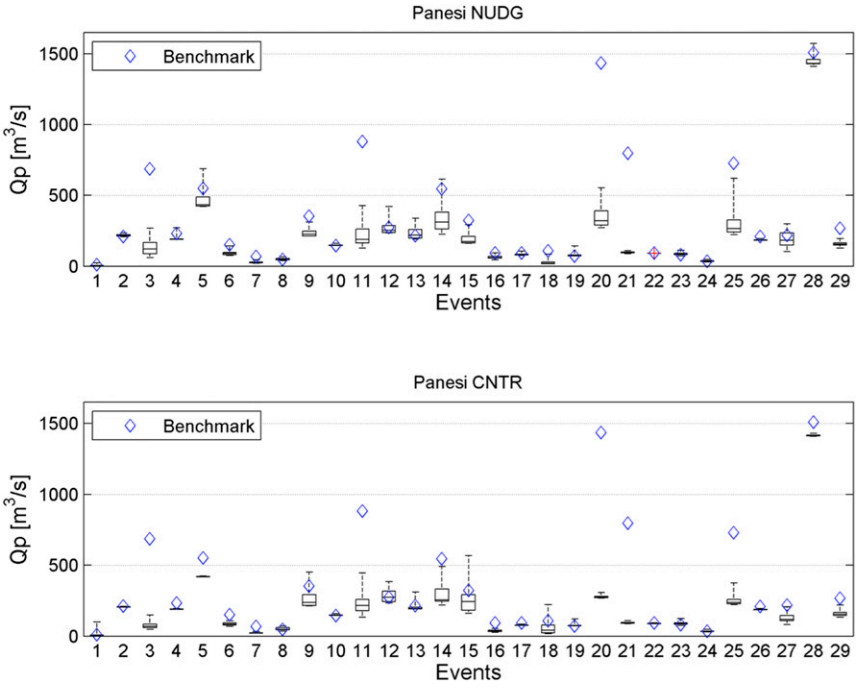

FIG. 9. Peak flows ($m^3 s^{-1}$) for the Entella basin at Panesi (364 km^2) for the reference hydrographs (blue diamonds) and produced by the forecasting chain (box plots). The progressive number identifying the forecast event is reported on the x axis. (top) The results with data assimilation in MOLOCH (NUDG experiments) and (bottom) the results using MOLOCH without data assimilation (CNTR runs).

systems develop using the available CAPE. Conversely, in November, strong large-scale forcing rapidly removes the ''perturbation'' imposed by the assimilation. Although during the assimilation period it is possible to trigger convection in the correct position, in the free forecast convection returns to its equilibrium with the synoptic-scale flow and all the modifications are lost rapidly.

The general picture provided by these results is in good agreement with the study by Craig et al. (2012). However, while they obtained a negligible correction in terms of location of the precipitation objects, our assimilation procedure systematically improves the position.

Finally, it is worth noting that in spite of the average behavior described, a single case study may deviate. As an example, the simulation of the first phase of the flood event occurring on the morning of 9 October 2014 can be classified, at least partly, as equilibrium convection with τ_c between 5 and 10 h (note that later in the afternoon the convective time scale increases, changing the convection regime in the second phase of the event). The impact of the nudging on rainfall forecasts is noticeable both at the end of the assimilation period (Figs. 8a–c) and 3 h later (Figs. 8d–f). It can be even noticed up to 9 h into the free forecast, at least as far as the amplitude A component of the SAL is concerned (not shown), thus much longer than expected.

c. *Hydrological impacts of rainfall assimilation in MOLOCH*

From the beginning of the hydrological model run to the end of the data assimilation period, the hydrological predictions are carried out using observations as input, while the meteorological variables provided by MOLOCH are used from the end of the assimilation period onwards. This configuration is implemented in order to mimic a possible practical application where, to feed the hydrological model, observations are preferred as long as available, and the main interest is in evaluating the forecast improvement after the assimilation period.

Since Continuum is a continuous hydrological model, the run can be initialized with the state variables estimated and saved during the 1-yr-long (2014) run; the latter is performed using the observations as input and produces the ''reference hydrographs.'' As described in section 3, the hydrological verification is carried out only for the experiments that apply a 6-h assimilation window, since it is the setup that leads to a larger and more long-lasting improvement in QPF. The precipitation

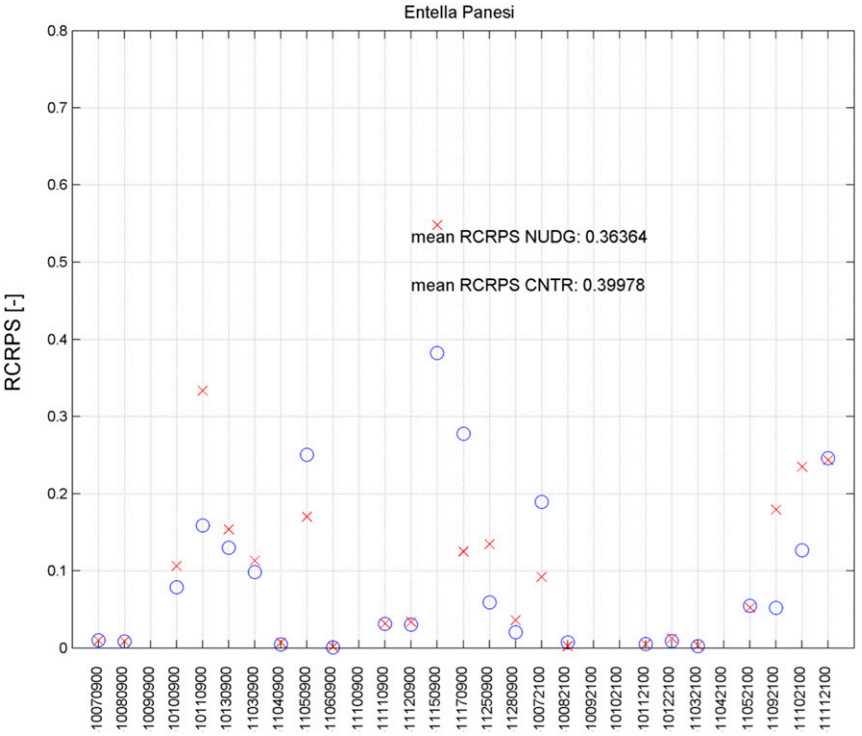

FIG. 10. RCRPS for the discharge simulations for the Entella basin at Panesi obtained using MOLOCH without data assimilation (CNTR; red crosses) and with data assimilation (NUDG; blue circles).

analysis (section 4a) demonstrates that the improvements in precipitation forecasts rapidly decrease after the first 3–6 h following the assimilation period, while the maximum response time of the catchments of the considered domain is around 8–10 h. As a consequence, it was decided to carry out the comparison in terms of peak flows in a time window that starts at the end of the assimilation period and lasts for 18 h. Since a meteorological analysis is already presented in section 4a, here results are not provided in terms of precipitation fields, but in terms of streamflow prediction, thus accounting for the nonlinear effects in the rainfall–runoff process.

Figures 9–12 show the results for two basins that belong to the considered study area, while Fig. 13 summarizes the results for all the 20 basins considered in this study. Figures 9 and 11 report on the x axis the progressive forecast number (forecasts listed in Table 1), while the corresponding peak flow value is on the y axis; blue diamonds represent the benchmark (reference hydrograph) while the box plots are built using the peak flows of the simulation ensemble. The top panel presents the results with data assimilation (NUDG) in MOLOCH, and the bottom panel presents those of the CNTR run. In some cases, the results are really similar and assimilation does not lead to any improvement, while in other cases the improvement is more evident, and the reference peak flow lays inside the whiskers or the edges of the box (25th and 75th percentiles), for example, as for events 5 and 28 in both basins. Finally, for some cases, the assimilation cannot completely correct the forecast, but it is able to improve it, as for events 20 and 25 in the Entella basin (Fig. 9), where nudging reduces the underestimation, and for event 11 in the Vara basin (Fig. 11), where nudging reduces the overestimation.

These results are corroborated by Figs. 10 and 12 that report the values of RCRPS for each event. There are some cases where RCRPS increases with nudging, although this occurs especially for those events characterized by pretty low peak flows. However, for many of the most intense events, RCRPS in NUDG decreases with respect to the CNTR run. The mean RCRPS calculated over all the events is lower for the NUDG runs with respect to the CNTR.

An analysis devoted to evaluate the timing of the peaks is not carried out since the results would not have been meaningful, as a consequence of the applied methodology and of the time/space scales involved in the present study. Indeed, RainFARM considers a reliable temporal scale T_{rel} of 6 h, which is of the same order of magnitude of the largest basin concentration time (which is around 10–12 h). Within the T_{rel} time

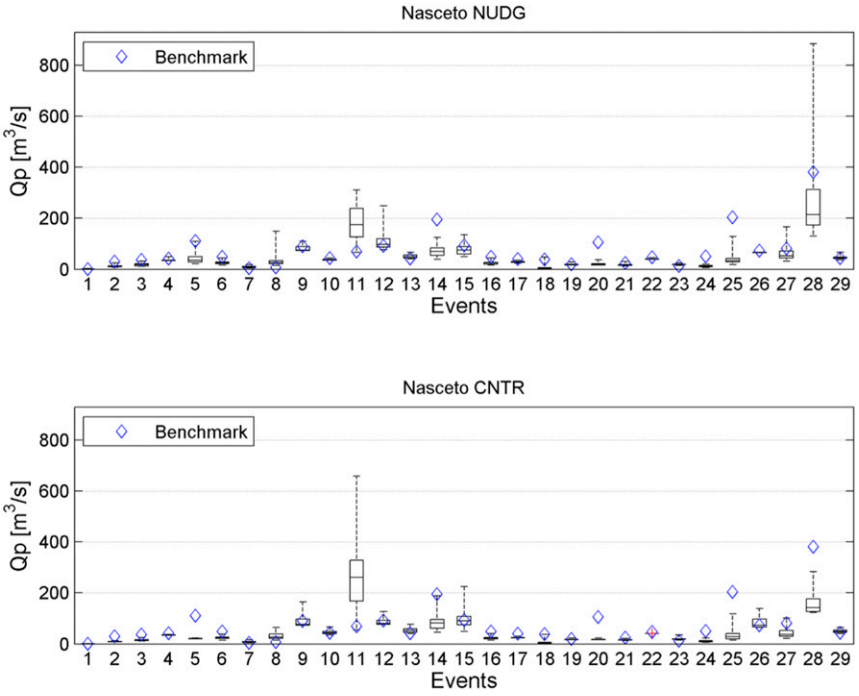

FIG. 11. As in Fig. 9, but for the Vara basin closed at Nasceto (202 km^2).

interval, the temporal sequence of the NWP rainfall fields is generally lost, since RainFARM randomly defines precipitation time sequences. The use of a stochastic downscaling model to produce rainfall scenarios allows us to deal with possible errors of localization and timing of precipitation forecasts, but does not allow us to detect any possible benefit in terms of timing of the streamflow. An analysis of discharge timing would have required a different approach, based on direct coupling between meteorological and hydrological models, which has to rely on very precise QPF from the NWP system. However, since the analyzed catchments are small, this is a very challenging task, especially beyond the nowcasting range, since rainfall forecast accuracy decreases very rapidly, due to limited predictability of convective phenomena.

Figure 13 shows the synthesis of the results for the 20 basins considered within the study area. For each basin, the mean RCRPS is computed over all the events in order to estimate the overall effects of data assimilation on a large number of simulations. The picture shows that there is an average tendency to improve the performance due to data assimilation even if it is not a very strong and systematic improvement for all of the basins. However, only 2 basins out of 20 show a nonnegligible worsening (Magra-Ameglia and Magra-Calamazza), while in some cases there is only a negligible difference between NUDG and CNTR experiments, either because data assimilation does not provide any relevant improvement or because the basin is not affected by rainfall and thus streamflow is low even in the reference hydrograph. In practice, the CNTR run correctly forecasts no rain and the NUDG run does not degrade the forecast, so that results are similar in terms of streamflow. It is worth noting that in cases of high flow, results are generally improved with the rainfall assimilation (NUDG experiments), as can be inferred by looking at the box plot of the single catchments; on the other hand, in cases characterized by no relevant flows, the assimilation does not generate artifacts or unexpected rainfall, and as a consequence, false streamflow events.

Finally, for the sake of completeness, the performance of the hydrological model evaluated during the period of interest, that is, from 7 October to 28 November 2014, is reported in Table 4, which shows the skill scores for the calibrated sections. Comparing score values in Table 2 and Table 4, it turns out that hydrological model performance during the period of analysis is on average worse than for the entire calibration period.

5. Conclusions

This study evaluates the impact of rainfall assimilation in a high-resolution convection-permitting model, performed through a simple nudging scheme that progressively modifies the specific humidity profiles of the

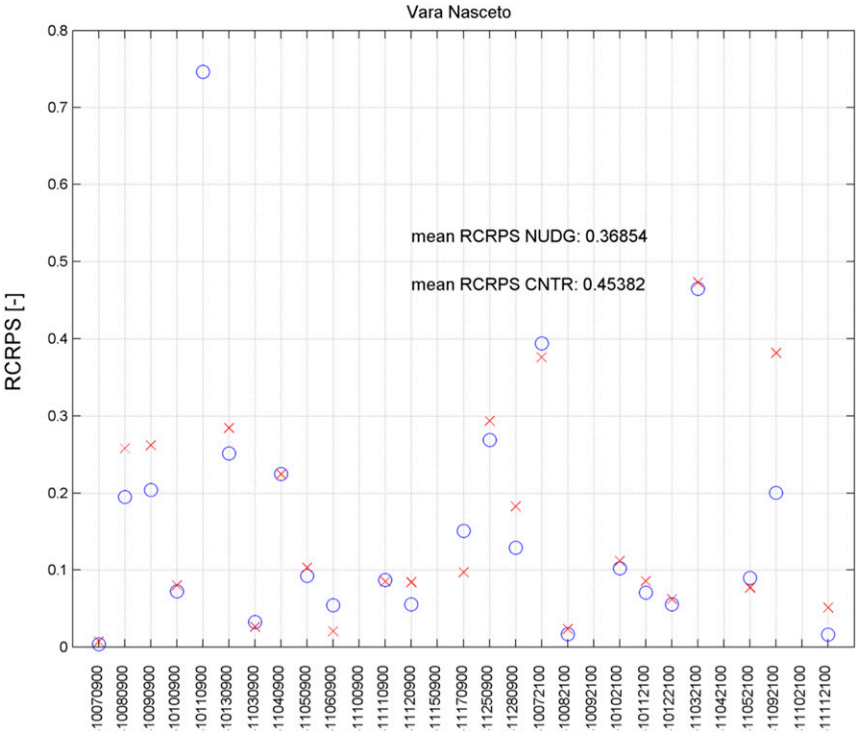

FIG. 12. As in Fig. 10, but for the Vara basin closed at Nasceto.

model. Assimilation of radar data at convective scales is a challenging issue, especially within the framework of real-time hydrometeorological predictions. However, most of the previous studies were devoted only to the evaluation of the meteorological aspects of data assimilation. Here, the assimilation scheme is developed and implemented in order to be feasible for operational activity, and it is evaluated not only in terms of QPF, but

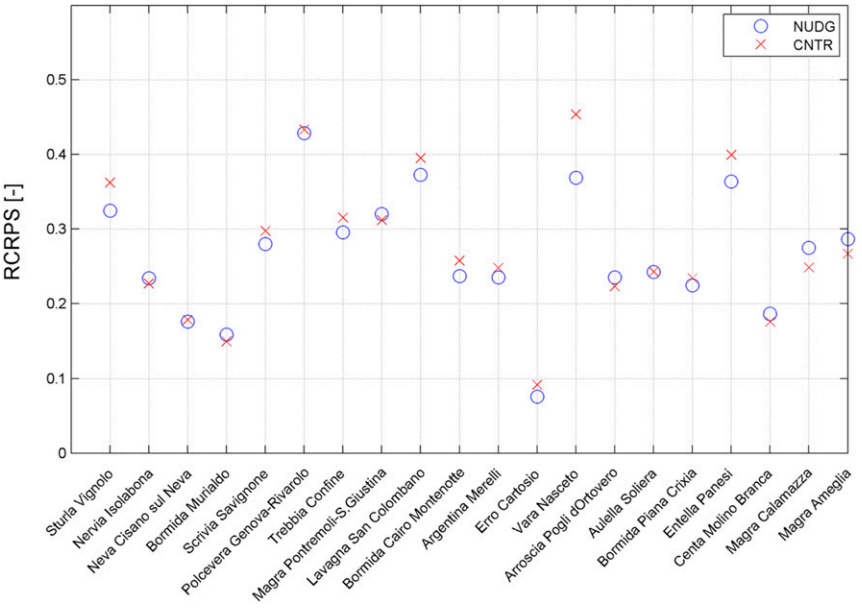

FIG. 13. Averaged RCRPS for all the events according to the basins and closure sections (on the *x* axis, ordered by catchment size) computed for the MOLOCH without data assimilation (CNTR; red crosses) and with data assimilation in MOLOCH (NUDG; blue circles).

TABLE 4. NS and REHS for the discharge simulations by Continuum model driven by observations during the period of interest (from 7 Oct to 28 Nov 2014) for different basins and sections.

Basin	Section	NS	REHF
Magra	Calamazza	0.62	0.35
Vara	Nasceto	0.66	0.32
Entella	Panesi	0.43	0.41
Bisagno	Passerella Firpo	0.18	0.36
Neva	Cisano	0.61	0.24
Arroscia	Pogli	0.66	0.63
Argentina	Merelli	0.73	0.42
Bormida	Murialdo	0.30	0.65
Bormida	Piana Crixia	0.44	0.43
Orba	Tiglieto	0.72	0.33
Aveto	Cabanne	0.45	0.56

also considering the hydrological response. To attain this aim, a complete hydrometeorological forecasting chain has been set up.

The evaluation of radar rainfall assimilation in the meteorological model MOLOCH, carried out using an object-oriented skill score (SAL), shows a positive impact, since the nudging scheme produces a systematic improvement of QPF, in terms of the location, intensity, and structure of the precipitation field. This should not be considered an a priori expected result since the nudging scheme, originally developed for a hydrostatic model and applied to large-scale precipitation systems, is adapted and implemented for the first time to convective scales. While a large improvement is observed during the assimilation, the benefit is limited to the first hours of the free forecast following the assimilation window. Nudging proves to be able to remove misplaced rainfall areas and to trigger precipitation systems in the correct place and at the right time. The latter characteristic is often associated with the activation of vertical motion due to latent heat release where saturation is reached and condensation occurs. Although the results suggest that this nudging application is limited to the nowcasting range, some benefits are appreciated also in the hydrological prediction, since for small basins such as those that characterize the Liguria region, even small corrections of QPF location and intensity may be critical. Finally, the experiments provide some relevant and practical indications on the frequency of the assimilated data and on the length of the assimilation period: the nudging scheme does not need high-frequency data (hourly data are suitable), and its results are much better when a 6-h interval is used for the assimilation (instead of 3 h only).

In addition, this study provides support to the results of Craig et al. (2012) that relate the impact of assimilation of rainfall radar estimates with the environment characteristics, since similar results are obtained here using a different convection-permitting model, a different nudging assimilation scheme, and a different and larger sample of forecasts of heavy precipitation events. Strong large-scale forcing and equilibrium convection limit the impact and duration of the improvement gained by the assimilation, since after the nudging period, the synoptic dynamics, which is almost unaffected by the assimilation, quickly regain control. Conversely, for nonequilibrium convection and weak large-scale forcing, the assimilation scheme shows larger improvements since it is effective in providing the local trigger for convection, which is the critical factor in order to attain accurate QPF under these environmental conditions.

The limited duration of the rainfall assimilation benefits is consistent with earlier studies (Dixon et al. 2009; Rossa et al. 2010; Sokol and Zacharov 2012; Tingwell 2012; Dow and Macpherson 2013; Korsholm et al. 2015) and can be ascribed partly to the very short time scales and low predictability of dynamics dominated by convective instability, and partly to the fact the nudging acts only indirectly on the dynamics itself, since it modifies humidity profiles, and can hardly modify the larger scales. Moreover, corrections are possible only in the area where precipitation is observed, and thus rainfall assimilation can be dependent on the initialization time of the forecast, with respect to the development of the precipitation system (Rossa et al. 2010). A possible way to reinforce the nudging results is to combine them with assimilation at the mesoscale of other observations. It has been shown that the assimilation of surface, satellite, aircraft, or radar data in addition to rainfall estimates can provide promising results (Dow and Macpherson 2013; Liu et al. 2013), since while nudging impacts the skill for very short lead times (3 h), additional high-resolution information can contribute to the skill even longer (Dixon et al. 2009). Along this line, a system for assimilating surface data provided by a local network of ground stations has already proved to be useful when applied to MOLOCH for heavy precipitation forecasts over Liguria (Tiesi et al. 2016). Therefore, this points toward a significant improvement of meteorological and hydrological predictions in the perspective of complementing the initialization with the assimilation of other variables.

Acknowledgments. This work was supported by the Italian Civil Protection Department, by the Liguria Region, and by the Italian CNR flagship project RITMARE. This work is a contribution to the HyMeX international program. We are very grateful to all the meteorologists and the hydrologists of the Meteo-Hydrologic Centre of Liguria Region for the many useful discussions we had and for providing technical reports of the severe weather events. We also thank

Prof. Silvana Di Sabatino, supervisor of Thomas Gastaldo's master's thesis at University of Bologna, and Dr. Michael Sprenger (ETH Zurich) for kindly providing the SAL code.

APPENDIX

Skill Scores for Hydrological Model Calibration

The performance of the calibrated parameter set was evaluated referring to some standard statistics used in hydrology, that is, the Nash–Sutcliffe (NS) coefficient (Nash and Sutcliffe 1970):

$$\mathrm{NS} = 1 - \sum_{t=1}^{t_{\max}} \frac{[Q_m(t) - Q_0(t)]^2}{[Q_m(t) - \overline{Q_0}]^2}$$

and the relative error of high flows:

$$\mathrm{REHF} = \frac{1}{t_{\max}} \left[\sum_{t=1}^{t_{\max}} \frac{|Q_m(t) - Q_0(t)|}{Q_0(t)} \right]_{Q>Q_{\mathrm{th}}},$$

where $t_{\max}$ is the number of instants of the simulations, $Q_m(t)$ and $Q_0(t)$ are the modeled and observed streamflows at time t, $\overline{Q_0}$ is the mean observed streamflow, and Q_{th} has been chosen as the 99th percentile of the observed hydrograph along the calibration period.

REFERENCES

Berenguer, M., C. Corral, R. Sanchez-Diesma, and D. Sempere-Torres, 2005: Hydrological validation of a radar-based nowcasting technique. *J. Hydrometeor.*, **6**, 532–549, doi:10.1175/JHM433.1.

Bick, T., and Coauthors, 2016: Assimilation of 3D radar reflectivities with an ensemble Kalman filter on the convective scale. *Quart. J. Roy. Meteor. Soc.*, **142**, 1490–1504, doi:10.1002/qj.2751.

Billett, S., and E. F. Toro, 1997: On WAF-type schemes for multidimensional hyperbolic conservation laws. *J. Comput. Phys.*, **130**, 1–24, doi:10.1006/jcph.1996.5470.

Boni, G., L. Ferraris, F. Giannoni, G. Roth, and R. Rudari, 2007: Flood probability analysis for un-gauged watersheds by means of a simple distributed hydrologic model. *Adv. Water Resour.*, **30**, 2135–2144, doi:10.1016/j.advwatres.2006.08.009.

Borga, M., 2002: Accuracy of radar rainfall estimates for streamflow simulation. *J. Hydrol.*, **267**, 26–39, doi:10.1016/S0022-1694(02)00137-3.

Buzzi, A., and S. Davolio, 2007: Modeling precipitation processes and data assimilation for NWP - Rainfall assimilation into limited area models. *Measuring Precipitation from Space—EURAINSAT and the Future*, V. Levizzani, P. Bauer, and F. J. Turk, Eds., Springer, 459–470.

——, M. D'Isidoro, and S. Davolio, 2003: A case study of an orographic cyclone south of the Alps during the MAP SOP. *Quart. J. Roy. Meteor. Soc.*, **129**, 1795–1818, doi:10.1256/qj.02.112.

——, S. Davolio, P. Malguzzi, O. Drofa, and D. Mastrangelo, 2014: Heavy rainfall episodes over Liguria of autumn 2011: Numerical forecasting experiments. *Nat. Hazards Earth Syst. Sci.*, **14**, 1325–1340, doi:10.5194/nhess-14-1325-2014.

Clark, P., N. Roberts, H. Lean, S. P. Ballard, and C. Charlton-Perez, 2016: Convection-permitting models: A step-change in rainfall forecasting. *Meteor. Appl.*, **23**, 165–181, doi:10.1002/met.1538.

Craig, G. C., C. Keil, and D. Leuenberger, 2012: Constraints on the impact of radar rainfall data assimilation on forecasts of cumulus convection. *Quart. J. Roy. Meteor. Soc.*, **138**, 340–352, doi:10.1002/qj.929.

Cuo, L., T. C. Pagano, and Q. J. Wang, 2011: A review of quantitative precipitation forecasts and their use in short- to medium-range streamflow forecasting. *J. Hydrometeor.*, **12**, 713–728, doi:10.1175/2011JHM1347.1.

Davolio, S., and A. Buzzi, 2004: A nudging scheme for the assimilation of precipitation data into a mesoscale model. *Wea. Forecasting*, **19**, 855–871, doi:10.1175/1520-0434(2004)019<0855:ANSFTA>2.0.CO;2.

——, F. Silvestro, and P. Malguzzi, 2015: Effects of increasing horizontal resolution in a convection permitting model on flood forecasting: The 2011 dramatic events in Liguria (Italy). *J. Hydrometeor.*, **16**, 1843–1856, doi:10.1175/JHM-D-14-0094.1.

——, A. Volontè, A. Manzato, A. Pucillo, A. Cicogna, and M. E. Ferrario, 2016: Mechanisms producing different precipitation patterns over north-eastern Italy: Insights from HyMeX-SOP1 and previous events. *Quart. J. Roy. Meteor. Soc.*, **142**, 188–205, doi:10.1002/qj.2731.

——, R. Henin, P. Stocchi, and A. Buzzi, 2017: Bora wind and heavy persistent precipitation: Atmospheric water balance and role of air–sea fluxes over the Adriatic Sea. *Quart. J. Roy. Meteor. Soc.*, **143**, 1165–1177, doi:10.1002/qj.3002.

Deidda, R., R. Benzi, and F. Siccardi, 1999: Multifractal modeling of anomalous scaling laws in rainfall. *Water Resour. Res.*, **35**, 1853–1867, doi:10.1029/1999WR900036.

Dickinson, R., 1988: The force-restore method for surface temperature and its generalization. *J. Climate*, **1**, 1086–1097, doi:10.1175/1520-0442(1988)001<1086:TFMFST>2.0.CO;2.

Dixon, M., Z. Li, H. Lean, N. Roberts, and S. Ballard, 2009: Impact of data assimilation on forecasting convection over the United Kingdom using a high-resolution version of the Met Office Unified Model. *Mon. Wea. Rev.*, **137**, 1562–1584, doi:10.1175/2008MWR2561.1.

Done, J. M., G. C. Craig, S. L. Gray, P. A. Clark, and M. E. B. Gray, 2006: Mesoscale simulations of organized convection: Importance of convective equilibrium. *Quart. J. Roy. Meteor. Soc.*, **132**, 737–756, doi:10.1256/qj.04.84.

Dow, G., and B. Macpherson, 2013: Benefit of convective-scale data assimilation and observing systems in the UK Models. Forecasting Research Technical Rep. 585, Met Office, 37 pp., http://www.metoffice.gov.uk/binaries/content/assets/mohippo/pdf/t/l/frtr585.pdf.

Ducrocq, V., and Coauthors, 2014: HyMeX-SOP1, the field campaign dedicated to heavy precipitation and flash flooding in the northwestern Mediterranean. *Bull. Amer. Meteor. Soc.*, **95**, 1083–1100, doi:10.1175/BAMS-D-12-00244.1.

Duffourg, F., and Coauthors, 2016: Offshore deep convection initiation and maintenance during the HyMeX IOP 16a heavy precipitation event. *Quart. J. Roy. Meteor. Soc.*, **142**, 259–274, doi:10.1002/qj.2725.

Emmanuel, K. A., 1994: *Atmospheric Convection.* Oxford University Press, 580 pp.

Faccini, F., F. Luino, A. Sacchini, and L. Turconi, 2015: The 4th October 2010 flash flood event in Genoa Sestri Ponente (Liguria, Italy). *Disaster Adv.*, **8** (8), 1–14.

Fiori, E., A. Comellas, L. Molini, N. Rebora, F. Siccardi, D. J. Gochis, S. Tanelli, and A. Parodi, 2014: Analysis and hindcast simulations of an extreme rainfall event in the Mediterranean area: The Genoa 2011 case. *Atmos. Res.*, **138**, 13–29, doi:10.1016/j.atmosres.2013.10.007.

——, L. Ferraris, L. Molini, F. Siccardi, D. Kranzlmueller, and A. Parodi, 2017: Triggering and evolution of a deep convective system in the Mediterranean Sea: Modelling and observations at a very fine scale. *Quart. J. Roy. Meteor. Soc.*, **143**, 927–941, doi:10.1002/qj.2977.

Giannoni, F., G. Roth, and R. Rudari, 2005: A procedure for drainage network identification from geomorphology and its application to the prediction of the hydrologic response. *Adv. Water Resour.*, **28**, 567–581, doi:10.1016/j.advwatres.2004.11.013.

Hersbach, H., 2000: Decomposition of the continuous ranked probability score for ensemble prediction systems. *Wea. Forecasting*, **15**, 559–570, doi:10.1175/1520-0434(2000)015<0559:DOTCRP>2.0.CO;2.

Kain, J. S., 2004: The Kain–Fritsch convective parameterization: An update. *J. Appl. Meteor.*, **43**, 170–181, doi:10.1175/1520-0450(2004)043<0170:TKCPAU>2.0.CO;2.

Keil, C., and G. C. Craig, 2011: Regime-dependent forecast uncertainty of convective precipitation. *Meteor. Z.*, **20**, 145–151, doi:10.1127/0941-2948/2011/0219.

——, F. Heinlein, and G. C. Craig, 2014: The convective adjustment time-scale as indicator of predictability of convective precipitation. *Quart. J. Roy. Meteor. Soc.*, **140**, 480–490, doi:10.1002/qj.2143.

Korsholm, U. S., C. Petersen, B. H. Sass, N. W. Nielsen, D. G. Jensen, B. T. Olsen, R. Gill, and H. Vedel, 2015: A new approach for assimilation of 2D radar precipitation in a high-resolution NWP model. *Meteor. Appl.*, **22**, 48–59, doi:10.1002/met.1466.

Laiolo, P., S. Gabellani, N. Rebora, R. Rudari, L. Ferraris, S. Ratto, H. Stevenin, and M. Cauduro, 2014: Validation of the Flood-PROOFS probabilistic forecasting system. *Hydrol. Processes*, **28**, 3466–3481, doi:10.1002/hyp.9888.

Lee, K.-O., C. Flamant, V. Ducrocq, F. Duffourg, N. Fourrié, and S. Davolio, 2016: Convective initiation and maintenance processes of two back-building mesoscale convective systems leading to heavy precipitation events in Southern Italy during HyMeX IOP 13. *Quart. J. Roy. Meteor. Soc.*, **142**, 2623–2635, doi:10.1002/qj.2851.

Leuenberger, D., and A. Rossa, 2007: Revisiting the latent heat nudging scheme for the rainfall assimilation of a simulated convective storm. *Meteor. Atmos. Phys.*, **98**, 195–215, doi:10.1007/s00703-007-0260-9.

Liu, J., M. Bray, and D. Han, 2013: A study on WRF radar data assimilation for hydrological rainfall prediction. *Hydrol. Earth Syst. Sci.*, **17**, 3095–3110, doi:10.5194/hess-17-3095-2013.

Malguzzi, P., G. Grossi, A. Buzzi, R. Ranzi, and R. Buizza, 2006: The 1966 "century" flood in Italy: A meteorological and hydrological revisitation. *J. Geophys. Res.*, **111**, D24106, doi:10.1029/2006JD007111.

Molini, L., A. Parodi, and F. Siccardi, 2009: Dealing with uncertainty: An analysis of the severe weather events over Italy in 2006. *Nat. Hazards Earth Syst. Sci.*, **9**, 1775–1786, doi:10.5194/nhess-9-1775-2009.

——, ——, N. Rebora, and G. C. Craig, 2011: Classifying severe rainfall events over Italy by hydrometeorological and dynamical criteria. *Quart. J. Roy. Meteor. Soc.*, **137**, 148–154, doi:10.1002/qj.741.

Morcrette, J.-J., H. W. Barker, J. N. S. Cole, M. J. Iacono, and R. Pincus, 2008: Impact of a new radiation package, McRad, in the ECMWF Integrated Forecasting System. *Mon. Wea. Rev.*, **136**, 4773–4798, doi:10.1175/2008MWR2363.1.

Nash, J. E., and J. V. Sutcliffe, 1970: River flood forecasting through conceptual models. Part I: A discussion of principles. *J. Hydrol.*, **10**, 282–290, doi:10.1016/0022-1694(70)90255-6.

Ramis, C., R. Romero, and V. Homar, 2009: The severe thunderstorm of 4 October 2007 in Mallorca: An observational study. *Nat. Hazards Earth Syst. Sci.*, **9**, 1237–1245, doi:10.5194/nhess-9-1237-2009.

Rebora, N., L. Ferraris, J. H. Hardenberg, and A. Provenzale, 2006: The RainFARM: Rainfall downscaling by a filtered auto regressive model. *J. Hydrometeor.*, **7**, 724–738, doi:10.1175/JHM517.1.

——, and Coauthors, 2013: Extreme rainfall in the Mediterranean: What can we learn from observations? *J. Hydrometeor.*, **14**, 906–922, doi:10.1175/JHM-D-12-083.1.

Ricard, D., V. Ducrocq, and L. Auger, 2012: A climatology of mesoscale environment associated with Mediterranean heavy precipitating events over northwestern Mediterranean area. *J. Appl. Meteor. Climatol.*, **51**, 468–488, doi:10.1175/JAMC-D-11-017.1.

Ritter, B., and J. F. Geleyn, 1992: A comprehensive radiation scheme for numerical weather prediction models with potential applications in climate simulations. *Mon. Wea. Rev.*, **120**, 303–325, doi:10.1175/1520-0493(1992)120<0303:ACRSFN>2.0.CO;2.

Röhner, L., K.-U. Nerding, and U. Corsmeier, 2016: Diagnostic study of a HyMeX heavy precipitation event over Spain by investigation of moisture trajectories. *Quart. J. Roy. Meteor. Soc.*, **142**, 287–297, doi:10.1002/qj.2825.

Rossa, A., P. Nurmi, and E. Ebert, 2008: Overview of methods for the verification of quantitative precipitation forecasts. *Precipitation: Advances in Measurement, Estimation and Prediction*, S. Michaelides, Ed., Springer, 419–452.

——, F. L. Del Guerra, M. Borga, F. Zanon, T. Settin, and D. Leuenberger, 2010: Radar-driven high-resolution hydro-meteorological forecasts of the 26 September 2007 Venice flash flood. *J. Hydrol.*, **394**, 230–244, doi:10.1016/j.jhydrol.2010.08.035.

Scheffknecht, P., E. Richard, and D. Lambert, 2016: A highly localized high-precipitation event over Corsica. *Quart. J. Roy. Meteor. Soc.*, **142**, 206–221, doi:10.1002/qj.2795.

Siccardi, F., G. Boni, L. Ferraris, and R. Rudari, 2005: A hydro-meteorological approach for probabilistic flood forecast. *J. Geophys. Res.*, **110**, D05101, doi:10.1029/2004JD005314.

Silvestro, F., N. Rebora, and L. Ferraris, 2011: Quantitative flood forecasting on small and medium size basins: A probabilistic approach for operational purposes. *J. Hydrometeor.*, **12**, 1432–1446, doi:10.1175/JHM-D-10-05022.1.

——, S. Gabellani, F. Giannoni, A. Parodi, N. Rebora, R. Rudari, and F. Siccardi, 2012: A hydrological analysis of the 4th November 2011 event in Genoa. *Nat. Hazards Earth Syst. Sci.*, **12**, 2743–2752, doi:10.5194/nhess-12-2743-2012.

——, ——, F. Delogu, R. Rudari, and G. Boni, 2013: Exploiting remote sensing land surface temperature in distributed hydrological modelling: The example of the Continuum model. *Hydrol. Earth Syst. Sci.*, **17**, 39–62, doi:10.5194/hess-17-39-2013.

——, ——, ——, ——, P. Laiolo, and G. Boni, 2015a: Uncertainty reduction and parameter estimation of a distributed hydrological model with ground and remote-sensing data. *Hydrol. Earth Syst. Sci.*, **19**, 1727–1751, doi:10.5194/hess-19-1727-2015.

——, N. Rebora, G. Cummings, and L. Ferraris, 2015b: Experiences of dealing with flash floods using an ensemble hydrological nowcasting chain: Implications of communication, accessibility and distribution of the results. *J. Flood Risk Manage.*, doi:10.1111/jfr3.12161, in press.

——, ——, F. Giannoni, A. Cavallo, and L. Ferraris, 2016: The flash flood of the Bisagno Creek on 9th October 2014: An ''unfortunate'' combination of spatial and temporal scales. *J. Hydrol.*, **541**, 50–62, doi:10.1016/j.jhydrol.2015.08.004.

Sinclair, S., and G. Pegram, 2005: Combining radar and rain gauge rainfall estimates using conditional merging. *Atmos. Sci. Lett.*, **6**, 19–22, doi:10.1002/asl.85.

Sokol, Z., 2009: Effects of an assimilation of radar and satellite data on a very short-range forecast of heavy convective rainfalls. *Atmos. Res.*, **93**, 188–206, doi:10.1016/j.atmosres.2008.11.001.

——, and P. Zacharov, 2012: Nowcasting of precipitation by an NWP model using assimilation of extrapolated radar reflectivity. *Quart. J. Roy. Meteor. Soc.*, **138**, 1072–1082, doi:10.1002/qj.970.

Stanki, H. R., L. J. Wilson, and W. R. Burrows, 1989: Survey of common verification methods in meteorology. WMO/TD 358, 114 pp.

Stephan, K., S. Klink, and C. Schraff, 2008: Assimilation of radar derived rain rates into the convective scale model COSMO-DE at DWD. *Quart. J. Roy. Meteor. Soc.*, **134**, 1315–1326, doi:10.1002/qj.269.

Sun, J., 2005: Convective-scale assimilation of radar data: Progress and challenges. *Quart. J. Roy. Meteor. Soc.*, **131**, 3439–3463, doi:10.1256/qj.05.149.

Tiesi, A., M. M. Miglietta, D. Conte, O. Drofa, S. Davolio, P. Malguzzi, and A. Buzzi, 2016: Heavy rain forecasting by model initialization with LAPS: A case study. *IEEE J. Sel. Top. Appl. Earth Obs. Remote Sens.*, **9**, 2619–2627, doi:10.1109/JSTARS.2016.2520018.

Tingwell, C., 2012: Observing system impact studies in ACCESS. Fifth WMO Workshop on the Impact of Various Observing Systems on Numerical Weather Prediction, Sedona, AZ, WMO, 34 pp., https://www.wmo.int/pages/prog/www/OSY/Meetings/NWP5_Sedona2012/2b2_Tingwell.pdf.

Trinh, B. N., J. Thielen-del Pozo, and G. Thirel, 2013: The reduction continuous rank probability score for evaluating discharge forecasts from hydrological ensemble prediction systems. *Atmos. Sci. Lett.*, **14**, 61–65, doi:10.1002/asl2.417.

Vieux, B. E., and P. B. Bedient, 2004: Assessing urban hydrologic prediction accuracy through event reconstruction. *J. Hydrol.*, **299**, 217–236, doi:10.1016/S0022-1694(04)00366-X.

Wernli, H., M. Paulat, M. Hagen, and C. Frei, 2008: SAL—A novel quality measure for the verification of quantitative precipitation forecasts. *Mon. Wea. Rev.*, **136**, 4470–4487, doi:10.1175/2008MWR2415.1.

——, C. Hofmann, and M. Zimmer, 2009: Spatial forecast verification methods intercomparison project: Application of the SAL technique. *Wea. Forecasting*, **24**, 1472–1484, doi:10.1175/2009WAF2222271.1.

Zampieri, M., P. Malguzzi, and A. Buzzi, 2005: Sensitivity of quantitative precipitation forecasts to boundary layer parameterization: A flash flood case study in the western Mediterranean. *Nat. Hazards Earth Syst. Sci.*, **5**, 603–612, doi:10.5194/nhess-5-603-2005.

Zimmer, M., G. C. Craig, C. Keil, and H. Wernli, 2011: Classification of precipitation events with a convective response timescale and their forecasting characteristics. *Geophys. Res. Lett.*, **38**, L05802, doi:10.1029/2010GL046199.